



HAL
open science

Study of gravity waves distribution and propagation in the thermosphere of Mars based on MGS, ODY, MRO and MAVEN density measurements

M. Vals, A. Spiga, F. Forget, E. Millour, L. Montabone, F. Lott

► To cite this version:

M. Vals, A. Spiga, F. Forget, E. Millour, L. Montabone, et al.. Study of gravity waves distribution and propagation in the thermosphere of Mars based on MGS, ODY, MRO and MAVEN density measurements. *Planetary and Space Science*, 2019, 178, pp.104708. 10.1016/j.pss.2019.104708 . hal-02967848

HAL Id: hal-02967848

<https://hal.sorbonne-universite.fr/hal-02967848v1>

Submitted on 15 Oct 2020

HAL is a multi-disciplinary open access archive for the deposit and dissemination of scientific research documents, whether they are published or not. The documents may come from teaching and research institutions in France or abroad, or from public or private research centers.

L'archive ouverte pluridisciplinaire **HAL**, est destinée au dépôt et à la diffusion de documents scientifiques de niveau recherche, publiés ou non, émanant des établissements d'enseignement et de recherche français ou étrangers, des laboratoires publics ou privés.

1 **Study of gravity waves distribution and propagation in the**
2 **thermosphere of Mars based on MGS, ODY, MRO and MAVEN**
3 **density measurements**

4 **M. Vals¹, A. Spiga^{1,2}, F. Forget¹, E. Millour¹, L. Montabone³, F. Lott¹**

5 ¹Laboratoire de Météorologie Dynamique (LMD/IPSL), Sorbonne Université, Centre National de la Recherche
6 Scientifique, École Normale Supérieure, École Polytechnique, Paris, France

7 ²Institut Universitaire de France, Paris, France

8 ³Space Science Institute, Greenbelt, MD, USA

9 **Key Points:**

- 10 • Gravity wave activity causes density perturbations in the Martian thermosphere.
- 11 • MAVEN found a correlation between gravity wave activity and inverse background
12 temperature.
- 13 • Lower-altitude aerobraking measurements do not show this correlation, except for
14 Mars Odyssey.
- 15 • Aerobraking data and climate models suggest instead wave activity correlated with
16 static stability.
- 17 • No such correlation in low latitudes points to a mix of saturation, critical levels and
18 sources.

Corresponding author: M. Vals, margaux.vals@lmd.jussieu.fr

Abstract

By measuring the regular oscillations of the density of CO₂ in the upper atmosphere (between 120 and 190 km), the mass spectrometer MAVEN/NGIMS (Atmosphere and Volatile Evolution/Neutral Gas Ion Mass Spectrometer) reveals the local impact of gravity waves. This yields precious information on the activity of gravity waves and the atmospheric conditions in which they propagate and break. The intensity of gravity waves measured by MAVEN in the upper atmosphere has been shown to be dictated by saturation processes in isothermal conditions. As a result, gravity waves activity is correlated to the evolution of the inverse of the background temperature. Previous data gathered at lower altitudes (~95 to ~150 km) during aerobraking by the accelerometers on board MGS (Mars Global Surveyor), ODY (Mars Odyssey) and MRO (Mars Reconnaissance Orbiter) are analyzed in the light of those recent findings with MAVEN. The anti-correlation between GW-induced density perturbations and background temperature is plausibly found in the ODY data acquired in the polar regions, but not in the MGS and MRO data. MRO data in polar regions exhibit a correlation between the density perturbations and the Brunt-Väisälä frequency (or, equivalently, static stability), obtained from Global Climate Modeling compiled in the Mars Climate Database. At lower altitude levels (between 100 and 120 km), although wave saturation might still be dominant, isothermal conditions are no longer verified. In this case, theory predicts that the intensity of gravity waves is no more correlated to background temperature, but to static stability. At other latitudes in the three aerobraking datasets, the GW-induced relative density perturbations are correlated with neither inverse temperature nor static stability; in this particular case, this means that the observed activity of gravity waves is not only controlled by saturation, but also by the effects of gravity-wave sources and wind filtering through critical levels. This result highlights the exceptional nature of MAVEN/NGIMS observations which combine both isothermal and saturated conditions contrary to aerobraking measurements.

1 Introduction

Gravity waves propagate as perturbations of the stratified atmospheric fluid [Gossard and Hooke, 1975], with the buoyancy force being the restoring mechanism giving rise to the waves [cf Fritts and Alexander, 2003; Alexander et al., 2010, for a review]. While being essentially regional-scale phenomena, gravity waves can be responsible for significant dynamical and thermal forcing of the global atmospheric state, as they transfer their momentum and

50 energy upon their saturation and breaking in the upper atmosphere [*Lindzen*, 1981; *Palmer*
51 *et al.*, 1986; *McFarlane*, 1987].

52 Gravity waves are ubiquitous in the Martian atmosphere and were actually one of the
53 first atmospheric phenomenon to be witnessed by orbiting spacecraft [*Briggs and Leovy*,
54 1974]. As is the case on Earth [*O'sullivan and Dunkerton*, 1995; *Vincent and Alexander*,
55 2000; *Plougonven et al.*, 2003; *Spiga et al.*, 2008], those waves may be triggered in the Mar-
56 tian lower atmosphere by different sources: topography [*Pickersgill and Hunt*, 1979, 1981],
57 convection [*Spiga et al.*, 2013; *Imamura et al.*, 2016], or jet-streams and fronts in ageostrophic
58 evolution. Amongst all those sources, only the impact of the topographic source on the global
59 circulation is accounted for in all Martian Global Climate Models [GCM, e.g. *Barnes*, 1990;
60 *Collins et al.*, 1997; *Forget et al.*, 1999; *Hartogh et al.*, 2005], although the exploration of the
61 impact of an additional non-orographic source is a topic of current active research [*Medvedev*
62 *et al.*, 2015; *Gilli et al.*, 2018].

63 The upward propagation of gravity waves from their tropospheric sources to the up-
64 per atmosphere leads to large departures of density, temperature and winds in the thermo-
65 sphere, owing to the exponential increase of gravity wave amplitude with height [*Fritts and*
66 *Alexander*, 2003; *Parish et al.*, 2009]. Measurements of CO₂ density through accelerome-
67 ters, gathered during the aerobraking of Mars Global Surveyor (MGS), Mars Odyssey (ODY)
68 and Mars Reconnaissance Orbiter (MRO) observed the sustained gravity wave activity in
69 the Martian thermosphere between 90 and 130 km [*Fritts et al.*, 2006; *Creasey et al.*, 2006;
70 *Tolson et al.*, 2007b]. Those measurements also demonstrated the large variability of the
71 gravity-wave amplitudes with season, local time, latitude and longitude.

72 The Mars Atmosphere and Volatile Evolution (MAVEN) mission to Mars [*Jakosky*
73 *et al.*, 2015], operating since 2014, is dedicated to studying the upper atmosphere of Mars
74 and, as such, is a unique opportunity to broaden the knowledge of gravity wave activity on
75 Mars. The mass spectrometer NGIMS (Neutral Gas Ion Mass Spectrometer) on board MAVEN
76 [*Mahaffy et al.*, 2015] recently delivered new and more accurate measurements of density
77 fluctuations at upper altitudes between 120 and 300 km, identified as typical gravity-wave
78 signatures [*Yiğit et al.*, 2015; *England et al.*, 2017].

79 Based on those MAVEN/NGIMS measurements, *Terada et al.* [2017] observed that
80 gravity-wave amplitudes derived from Ar density with wavelengths between ~100 and ~500 km
81 near the exobase in the Martian thermosphere are anti-correlated with the background tem-

82 perature. The authors demonstrated this anti-correlation by considering gravity waves satu-
83 ration caused by convective instability in the upper thermosphere. These observations were
84 further discussed in a recent study focusing on Ar density between 120 and 200 km by *Siddle*
85 *et al.* [2019], who observed that gravity waves amplitudes also increase with increasing solar
86 zenith angle.

87 The goal of this paper is to build on those recent findings by MAVEN and to expand
88 this analysis by comparing all available aerobraking data from other orbiting spacecraft. In
89 particular, we explore the saturation conditions of gravity waves in a lower part of the ther-
90 mosphere (between 90 and 130 km) than the one observed by MAVEN (between 120 and
91 300 km). Thus, we obtain a broader dataset of the variability of gravity wave activity with
92 altitude, latitude and season. This allows us to compare the available measurements with di-
93 agnostics obtained by GCM through the Mars Climate Database [MCD *Lewis et al.*, 1999;
94 *Forget et al.*, 1999; *Millour et al.*, 2015]

95 This paper is organized as follows. In section 2, we provide information on the datasets.
96 Section 3 features a discussion of the MAVEN/NGIMS measurements, while section 4 fea-
97 tures a comparative discussion of the aerobraking datasets. We conclude in section 5.

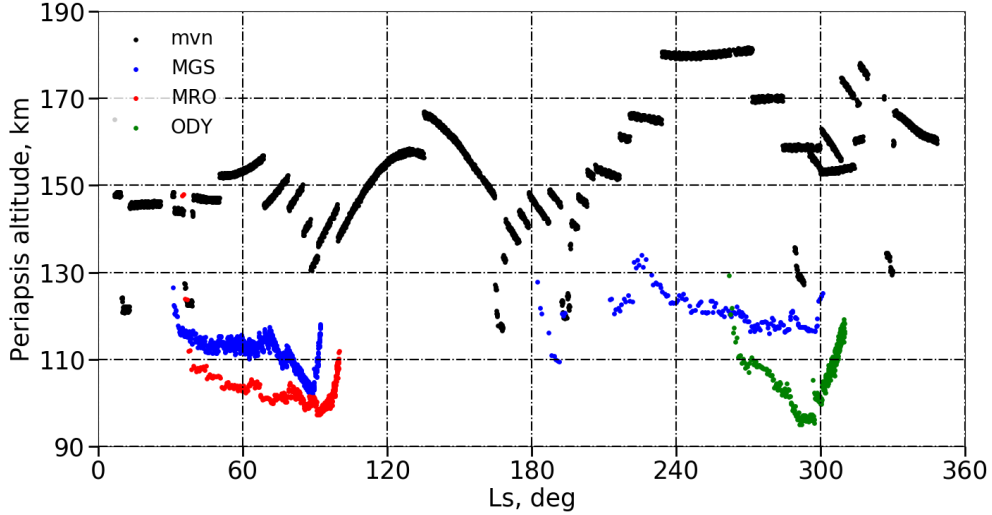
98 **2 Data and Method**

99 **2.1 Datasets used in this study**

100 During aerobraking operations in the Martian thermosphere, the accelerometers of
101 MGS, ODY and MRO [*Lyons et al.*, 1999; *Smith and Bell*, 2005; *Tolson et al.*, 2008] ac-
102 quired data during 850 passes for MRO (since September 1997, Martian Year [MY] 23)
103 [*Keating et al.*, 2002], 320 passes for ODY (since October 2001, MY 25) [*Tolson et al.*,
104 2007a], and 430 passes for MGS (from April to August 2006, MY 28) [*Tolson*, 2007], cov-
105 ering latitude ranges from 60°N to 90°S for MGS, 30°N to 90°N for ODY, and 0° to 90°S for
106 MRO. Periapsis altitudes varied from about 95 km to 150 km (see Figures 1 and 2).

107 In addition to those aerobraking datasets, the CO₂ density variations from 3124 orbits
108 are available from MAVEN/NGIMS mass spectrometer data reported in the NASA Plan-
109 etary Data System from October 2014 (MY32) to February 2017 (MY33) [*Benna and Ly-*
110 *ness*, 2014]. Considering the NGIMS settings were changed to a new operating mode start-
111 ing from February 2015, as mentioned in *England et al.* [2017] and *Terada et al.* [2017], we
112 chose to focus on datasets from February 2015 to February 2017. The instrument is still in

113 operation at the time of writing and the present study can be complemented in the future
 114 by an analysis of the interannual variability. The MAVEN observations cover (high periap-
 115 sis) altitude ranges between ~ 120 km and ~ 190 km, and have large latitudinal coverage, as
 116 shown in Figure 1 and Figure 2.

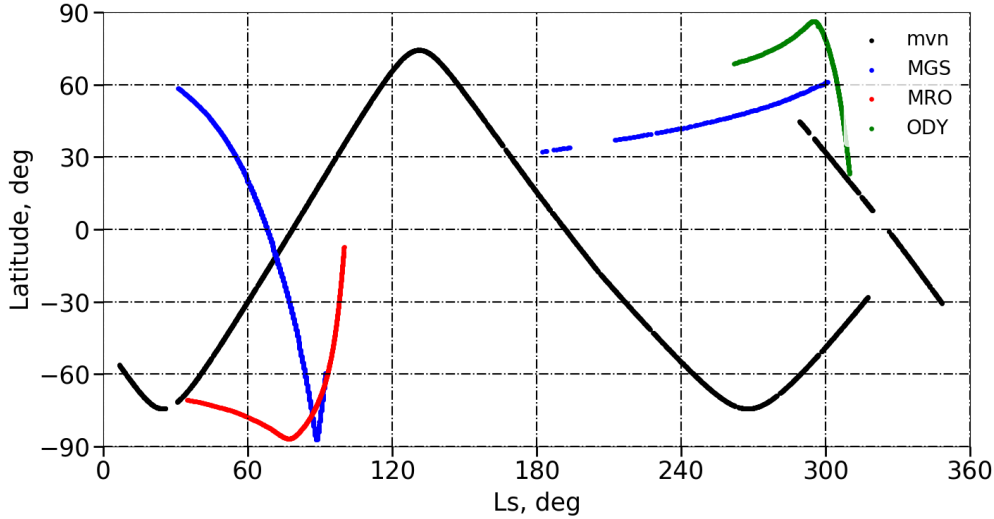


117 **Figure 1.** Vertical (km) and seasonal (Solar Longitude in degrees) coverage of Mars Global Surveyor
 118 (MGS), Mars Odyssey (ODY), Mars Reconnaissance Orbiter (MRO) and MAVEN (MVN) spacecrafts, each
 119 dot corresponds to the periapsis location of one orbit

123 2.2 Computing the amplitude of gravity wave perturbations

124 Along each orbit trajectory, we extract the longitudes, latitudes, solar longitudes (L_s ,
 125 which is the position of the planet on its orbit, defined as an angle from a reference posi-
 126 tion, corresponding by convention to the northern spring equinox), local times, altitudes,
 127 CO_2 density measurements, as well as the elapsed time from the periapsis. The geodesic
 128 distance from the periapsis is calculated from the latitude and longitude displacements. A
 129 relative density perturbation $\delta\rho_r$ is obtained by subtracting the mean density ρ_m [considered
 130 here to be a 40-second rolling averaged density, as in *Tolson et al.*, 1999, 2005, 2007b, 2008;
 131 *Creasey et al.*, 2006] from the instantaneous density ρ_i , and by normalizing with the mean
 132 density

$$\delta\rho_r = \frac{\rho_i - \rho_m}{\rho_m} \quad (1)$$

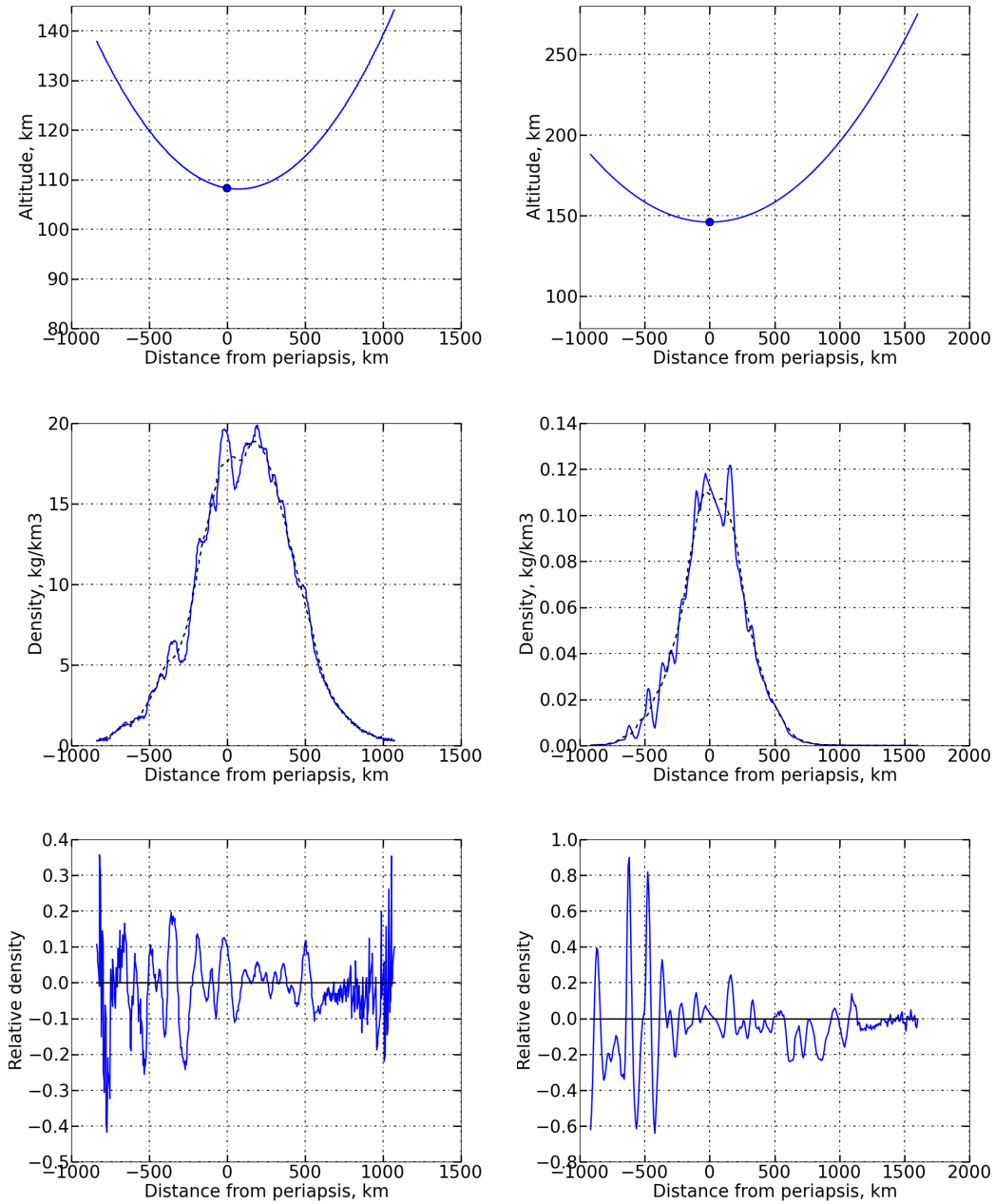


120 **Figure 2.** Latitudinal (degrees) and seasonal (Solar Longitude in degrees) coverage of Mars Global Sur-
 121 veyor (MGS), Mars Odyssey (ODY), Mars Reconnaissance Orbiter (MRO) and MAVEN (MVN) spacecrafts,
 122 each dot corresponds to the periapsis location of one orbit

133 Typical examples of orbit trajectory, absolute and relative density variations, obtained for the
 134 MGS orbit 1046 and for the MAVEN orbit 3641 are shown in Figure 3. Considering the rel-
 135 ative density perturbations, rather than the absolute value, enables a direct diagnostic of the
 136 effect of gravity waves, with the underlying assumption that the 40-second average provides
 137 an acceptable estimate of the “background” atmospheric state upon which the gravity waves
 138 propagate.

143 In order to quantify the amplitude (i.e. the intensity) of the observed gravity waves on
 144 a single orbit, and to assess the spatial and seasonal variability of the gravity wave activity,
 145 we calculate for each orbit the Root Mean Square (RMS) of the fluctuations of relative densi-
 146 ties $\delta\rho_r$ along the trajectory.

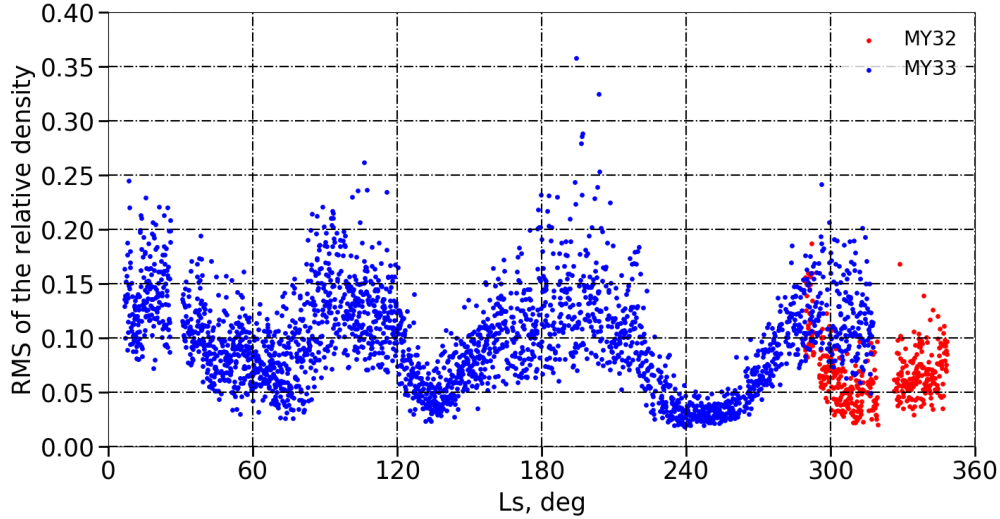
147 Figure 4 (MAVEN/NGIMS data) and Figure 5 (aerobraking data) show the seasonal
 148 variations of the GW activity as quantified by this RMS quantity, i.e. the RMS as a function
 149 of the L_s , all other parameters (longitudes, latitudes, local times, altitudes) confounded. A
 150 distinctive pattern of amplitude fluctuations with season is found in the MAVEN data in Fig-
 151 ure 4, in agreement with the tendencies discussed in *Terada et al.* [2017].



139 **Figure 3.** Left: example of orbit 1046 from MGS, Right: example of orbit 3641 from MAVEN. From Left
 140 to Right: orbit's trajectory characterized by the displacement in altitude along the distance from periapsis in
 141 km; Density variations in kg km^{-3} in function of the distance from periapsis in km ; Relative density variation
 142 in function of the distance from periapsis in km.

162 2.3 Temperature estimates

163 The background temperature T is estimated at each point of each orbit with the ideal
 164 gas law and the hydrostatic equilibrium, as a function of the mean density of CO_2 ρ and the



152 **Figure 4.** Seasonal variability of GWs amplitudes measured by MAVEN/NGIMS. Each point corresponds
 153 to the RMS of the relative densities calculated over each orbit. In this figure the RMS has been calculated on
 154 the points around the periapsis, where the trajectory is close to be horizontal, at distances from the periapsis
 155 comprised between -700 and 700 km. This restriction reduces the altitude range to around 15 km above the
 156 periapsis. Data gathered from Martian Year (MY) 32 are in red, and data from MY33 in blue.

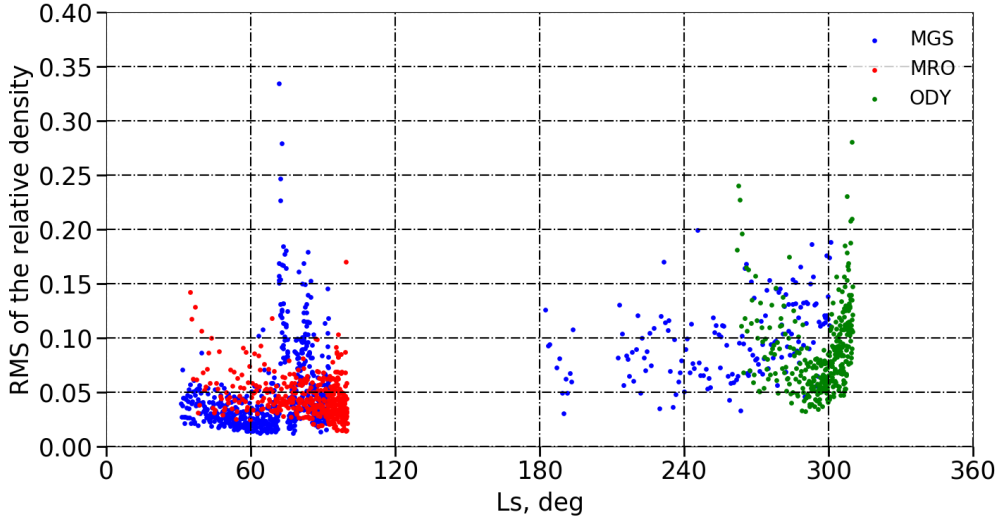
165 altitude z as follows:

$$\int \frac{\partial \rho}{\rho} = -\frac{g}{R_{CO_2} T} \int \partial z \quad (2)$$

166 with g the gravitational acceleration and R_{CO_2} the ideal gas constant of CO_2 .

167 We split the orbit in three parts.

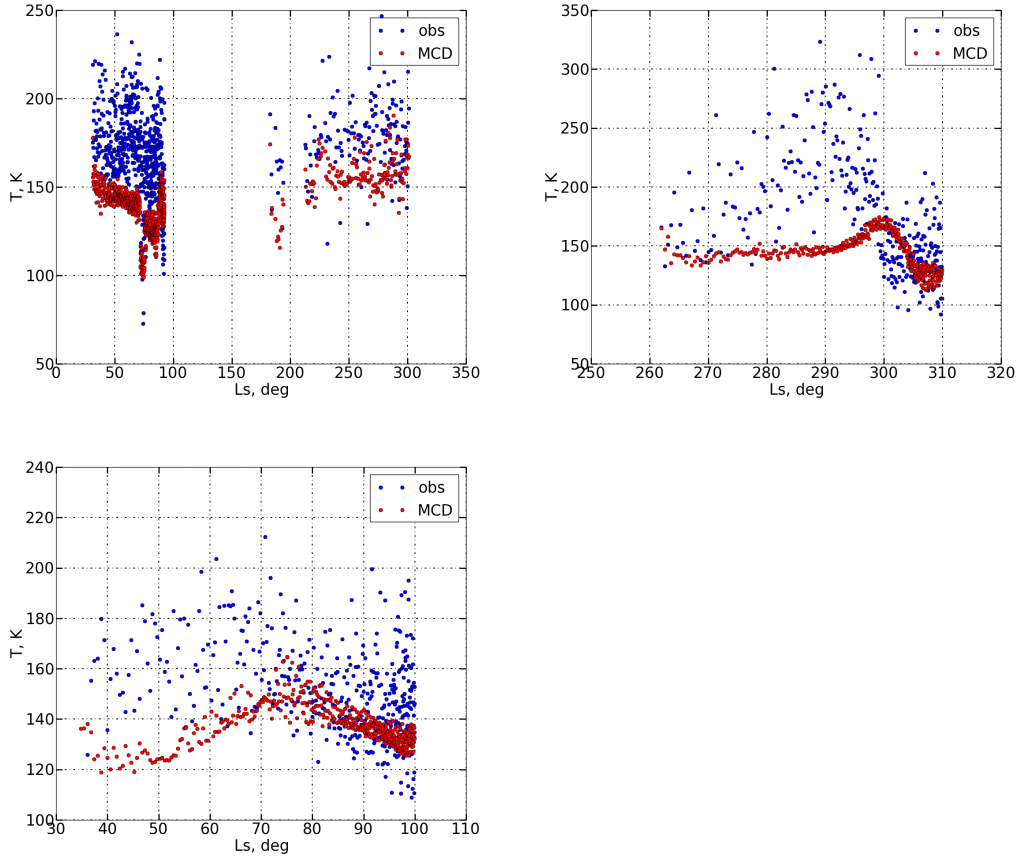
- 168 1. The middle leg is the part of the orbit track close to the periapsis, where the displace-
 169 ment is almost horizontal, the density almost constant, and, consequently, where the
 170 temperature can no longer be deduced from equation 2. We arbitrarily define this
 171 middle leg as containing the points for which the ratio between the mean density and
 172 the maximal density is greater than 10%.
- 173 2. The inbound leg corresponds to the points located "before" the periapsis not included
 174 in the middle leg.
- 175 3. The outbound leg refers to the points located "after" the periapsis not included in the
 176 middle leg.



157 **Figure 5.** Seasonal variability of GWs amplitudes measured by aerobraking instruments MGS, ODY and
 158 MRO. Each point corresponds to the RMS of the relative densities calculated over each orbit. In this figure
 159 the RMS has been calculated on the points around the periapsis, where the trajectory is close to be horizontal,
 160 at distances from the periapsis comprised between -400 and 400 km. Beyond these distances the aerobraking
 161 data become very noisy. This restriction reduces the altitude range to around 10 km above the periapsis.

177 Thus the middle leg of the measurements is excluded from the comparative analysis, and
 178 we only keep the inbound and outbound profiles for all aerobrakings and MAVEN/NGIMS
 179 measurements.

180 We found that in the inbound and outbound legs, the temperature profiles follow a sim-
 181 ilar vertical gradient. We thus study the variability of temperature from one orbit to another
 182 with a single representative value for both the inbound and outbound legs, chosen as the aver-
 183 age value on each leg. Those temperatures estimated from aerobraking and MAVEN/NGIMS
 184 measurements are compared in Figure 6 and Figure 7 with the temperature in the Mars Cli-
 185 mate Database [built from Global Climate Model (GCM) simulations *Millour et al., 2015*]
 186 for the same spatio-temporal coordinates (L_s , longitude, latitude, altitude, local time). Only
 187 the comparisons of temperatures measured on outbound legs versus temperature modeled in
 188 the MCD are displayed for the sake of brevity; the analysis for inbound legs is similar. The
 189 MCD temperatures are systematically lower than those observed by MAVEN and aerobrak-
 190 ing, and there is also much more variability in the observation data points; however, the over-
 191 all seasonal variability is well reproduced, except the $L_s = 290^\circ$ maximum observed by ODY.

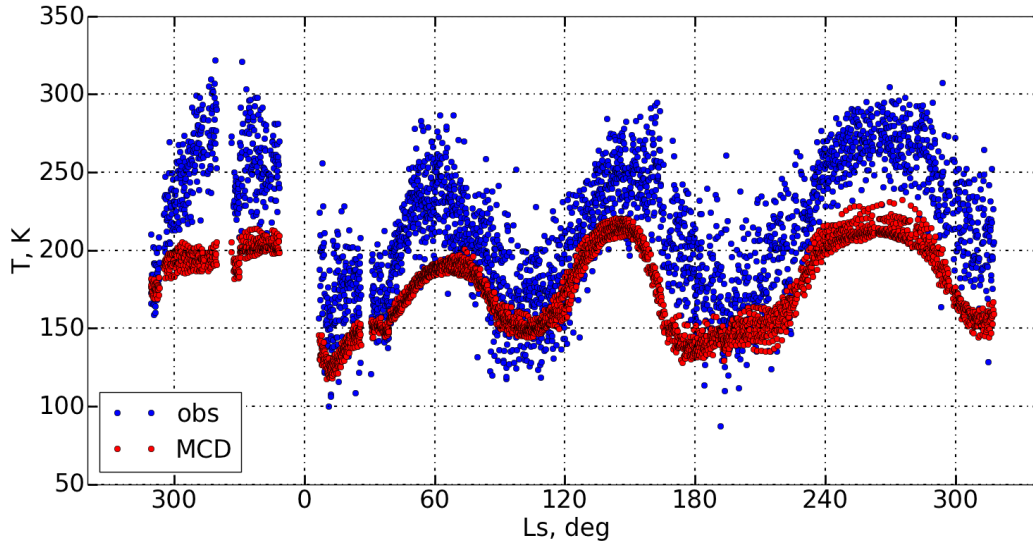


195 **Figure 6.** Mean background temperature estimated over the outbound leg and calculated from the CO₂
 196 density observations (blue dots) and estimated with the MCD (red dots) as a function of Solar Longitude;
 197 from the upper to the lower : MGS, ODY and MRO

192 This gives us confidence that using a value of background temperature averaged over the in-
 193 bound and outbound legs is suitable to carry out an analysis of the seasonal (climatological)
 194 trends.

201 **3 Vertical Propagation of Gravity Waves: analysis of the MAVEN observations in**
 202 **the thermosphere**

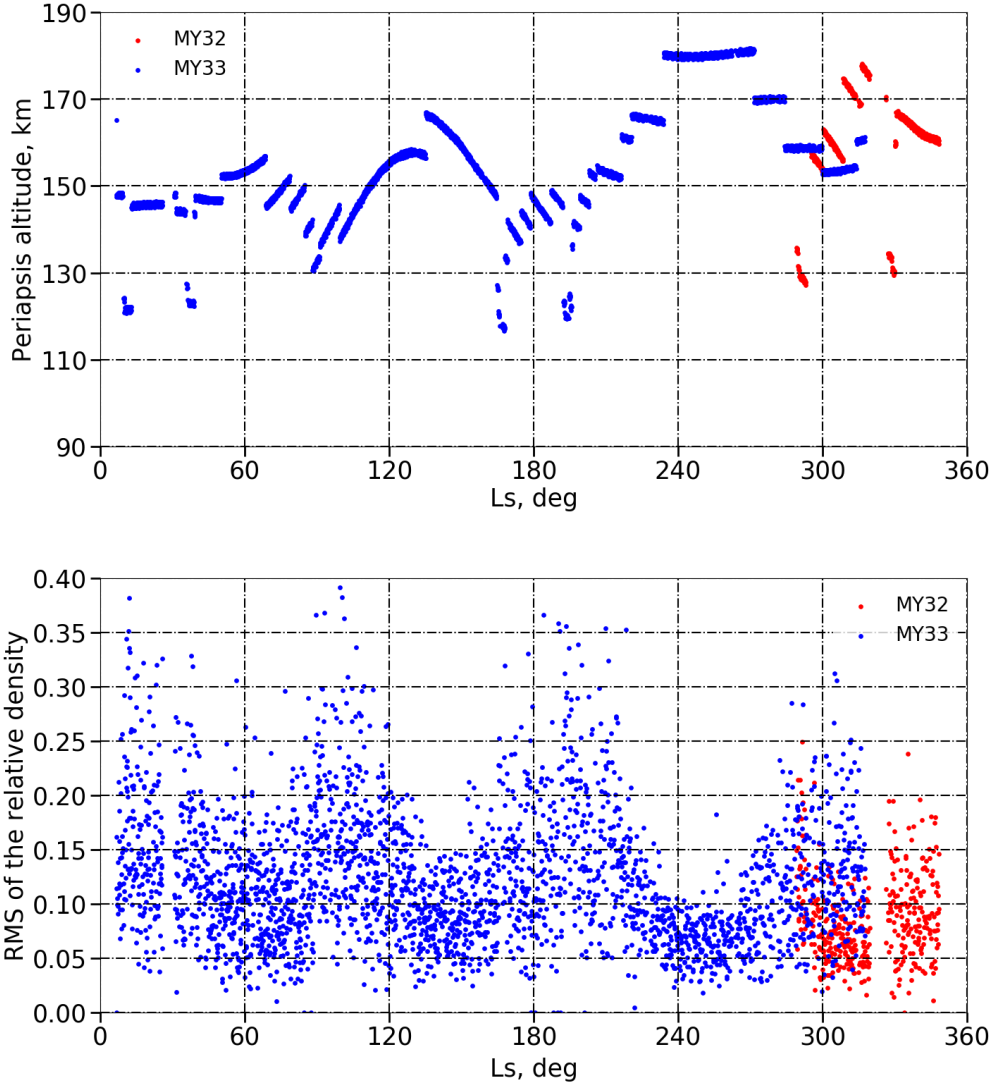
203 In the absence of additional wave sources and dissipation processes [e.g., radiative
 204 damping *Eckermann et al., 2011*], the amplitude of gravity waves is expected to grow ex-
 205 ponentially with altitude as the atmospheric density decreases. Conversely, the amplitudes of
 206 gravity waves appear to anti-correlate with altitude, according to the altitudes of the MAVEN
 207 measurements shown in Figure 1 and the amplitudes $\delta\rho$ of the perturbations shown in Fig-



198 **Figure 7.** Mean background temperature estimated over the outbound leg and calculated from the CO₂
 199 density observations of NGIMS instrument (blue dots) and estimated with the MCD (red dots) as a function of
 200 Solar Longitude

208 ure 4. In other words, in the MAVEN observations, gravity-wave amplitude seems to corre-
 209 late with density, as opposed to an anti-correlation expected if the amplification of gravity-
 210 wave amplitude with altitude (and reduced density) was the only controlling factor. This is
 211 confirmed by considering the seasonal variations of density perturbations $\delta\rho$ at a constant
 212 pressure level, e.g. at pressures $4 \times 10^{-8} < P < 6 \times 10^{-8}$ Pa (corresponding to altitudes
 213 between ~ 160 and ~ 240 km) in Figure 8. The observed variability in gravity-wave amplitude
 214 must be controlled by either the sources of those waves and/or the impact of saturation and
 215 critical levels.

221 In the MAVEN measurements, gravity wave activity in the thermosphere is randomly
 222 distributed with longitude and latitude (figures not shown). No correlation appears to exist
 223 between this gravity wave activity and either the position of topographical highs and lows
 224 (mountains and craters), or the position of mesospheric jet-streams. This suggests that the
 225 regional distribution of the intensity of gravity waves is more controlled by propagation ef-
 226 fects [e.g., filtering by saturation or critical levels, *Fritts and Alexander, 2003*] than by the
 227 distribution of the sources triggering those waves.



216 **Figure 8.** Upper: Vertical (km) and seasonal (Solar Longitude in degrees) coverage of MAVEN (MVN)
 217 spacecraft, each dot corresponds to the periapsis location of one orbit. Down: Seasonal variability of GWs
 218 amplitudes measured by MAVEN/NGIMS at a constant pressure level P such as $4 \times 10^{-8} < P < 6 \times 10^{-8}$ Pa.
 219 Each point corresponds to the RMS of the relative densities calculated over each orbit. Data gathered from
 220 Martian Year (MY) 32 are in red, and data from MY33 in blue.

228 The background horizontal wind plays a particularly crucial role in impacting the condi-
 229 tions for the upward propagation of gravity waves emitted in the troposphere. A critical
 230 level occurs when and where the background horizontal wind velocity \bar{u} almost equals the
 231 gravity wave phase speed c [first Eliassen-Palm theorem, *Lindzen*, 1981]. A gravity wave

232 that reaches a critical level can no longer propagate towards the thermosphere: hence hor-
 233 izontal circulations may filter out gravity waves emitted in the troposphere from the meso-
 234 sphere and the thermosphere.

235 Considering, for the sake of simplicity, a gravity-wave phase speed $c = 0$ (typical of
 236 orographic gravity waves), we explored the regional and seasonal variability of background
 237 horizontal winds \bar{u} simulated in the MCD from the troposphere to the lower mesosphere
 238 (since no measurements of such winds are available). We found no correlation between this
 239 variability, and the regional and seasonal variability of the gravity wave amplitudes observed
 240 by MAVEN (not shown). While the modeled winds have not been validated and may differ
 241 from reality, there is no reason to explain the variability of the observed gravity wave ampli-
 242 tudes solely with the occurrence of critical levels.

243 It follows from the above discussions that the most likely possibility to explain the
 244 observed variability of gravity wave amplitude in the MAVEN observations is the break-
 245 ing/saturation due to convective instability. This shall lead to, according to *Terada et al.*
 246 [2017], the gravity wave amplitudes to be inversely proportional to the background temper-
 247 ature. Let us propose an alternate, yet equivalent, derivation of the theoretical arguments in
 248 *Terada et al.* [2017] that we will use in section 4.

249 The saturation of a gravity wave occurs as soon as it encounters convective instability
 250 [Lindzen, 1981; Hauchecorne et al., 1987; Terada et al., 2017]. Local mixing occurs as the
 251 gravity wave breaks, inducing an adiabatic (neutral) temperature lapse rate. We consider the
 252 case of a medium-frequency gravity wave $f \ll \omega \ll N$, where f , ω and N are respectively
 253 the Coriolis, the gravity-wave and the Brunt-Väisälä frequencies, with N such that

$$N^2 = \frac{g}{T} \left[\frac{\partial T}{\partial z} + \frac{g}{C_p} \right]$$

254 assuming the short-wavelength approximation $2Hk_z \gg 1$, where k_z is the vertical wave
 255 number. Which are reasonable assumptions for most gravity waves observed in planetary up-
 256 per atmospheres [Fritts and Alexander, 2003]. In those conditions, according to *Hauchecorne*
 257 *et al.* [1987], the saturated conditions lead to

$$k_z \theta'_s = \frac{N^2 \bar{\theta}}{g} \quad \Rightarrow \quad \frac{\theta'_s}{\theta} = \frac{N^2}{gk_z} \quad (3)$$

258 where θ'_s is the amplitude of the wave at saturation (expressed in perturbations of potential
 259 temperature), $\bar{\theta}$ the background potential temperature and g the acceleration of gravity. Be-
 260 sides, the linearized fluid equations applied to the propagation of gravity waves [Fritts and

261 *Alexander, 2003*] lead to:

$$\frac{\theta'}{\bar{\theta}} = \frac{1}{c_s^2} \frac{P'}{\bar{\rho}} - \frac{\rho'}{\bar{\rho}} \quad (4)$$

262 where ρ is the density, P' and ρ' the pressure and density perturbations, and c_s the sound
 263 speed. We can neglect the compressibility term related to the background density gradient,
 264 which is equivalent to filter out acoustic gravity waves ($c_s \rightarrow \infty$). This entails:

$$\left| \frac{\rho'}{\bar{\rho}} \right| = \left| \frac{\theta'}{\bar{\theta}} \right| \quad (5)$$

265 Combining equations 3 and 5, we obtain the equation expressing the relative density pertur-
 266 bations by gravity waves:

$$\delta\rho = \frac{|\rho'|}{\bar{\rho}} = \frac{N^2}{k_z g} \quad (6)$$

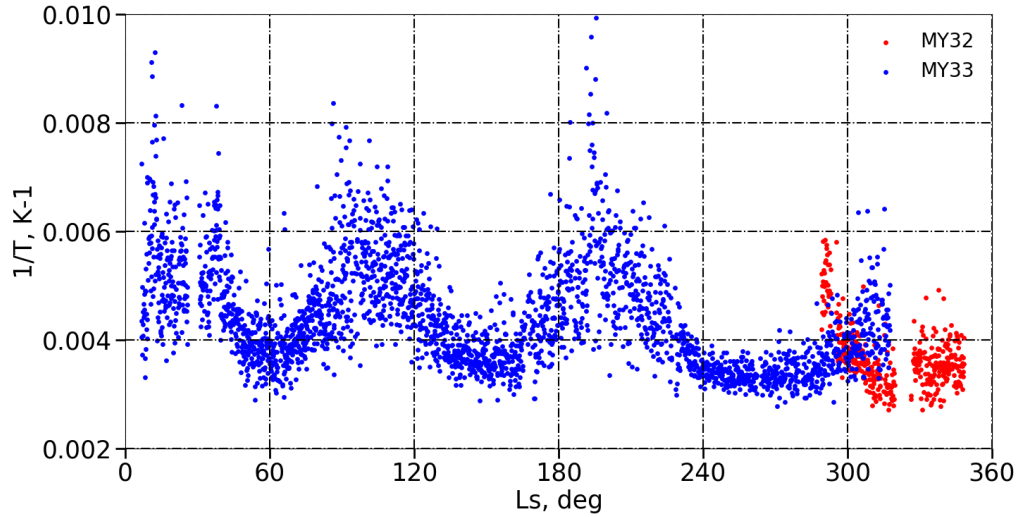
267 which corresponds to the observed diagnostic described in equation 1. Isothermal back-
 268 ground profiles $T = T_0$ are often observed in the Martian thermosphere, where EUV heating
 269 is offset by molecular conduction [*Bougher et al., 1990*]. In the specific case of isothermal
 270 profiles, N^2 can be reduced to:

$$N^2 = \frac{g}{\bar{\theta}} \frac{d\bar{\theta}}{dz} = \frac{g^2}{C_p T_0} \quad (7)$$

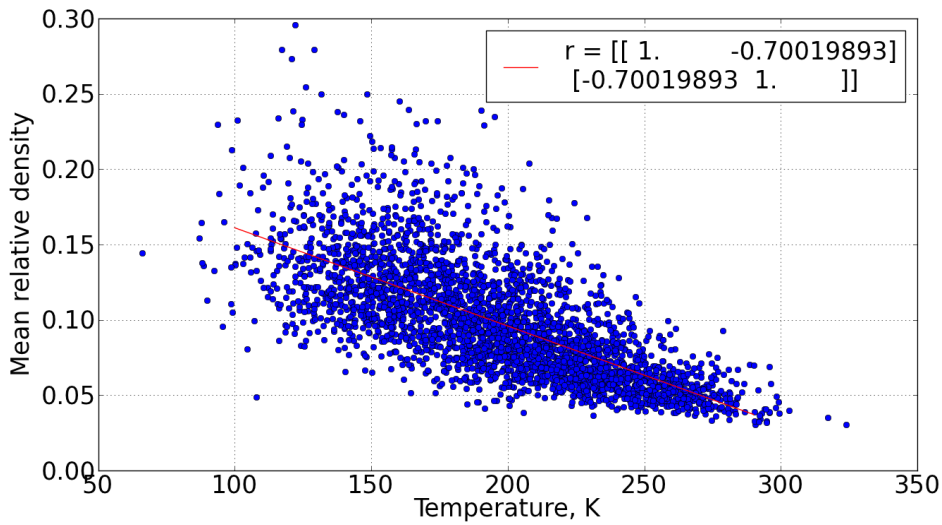
271 which yields the “inverse temperature” dependency [*Terada et al., 2017*] in the case of isother-
 272 mal profiles at saturation:

$$\delta\rho = \frac{|\rho'|}{\bar{\rho}} = \frac{g}{k_z C_p T_0} \quad (8)$$

273 MAVEN data are acquired high in the Martian thermosphere (above 150 km) even
 274 for deep dip acquisitions: hence the temperature profiles retrieved by MAVEN are approx-
 275 imately isothermal [*England et al., 2017; Terada et al., 2017*]. The temperature profiles mod-
 276 eled and compiled in the MCD also indicate widespread isothermal profiles at the altitudes
 277 probed by MAVEN. Comparing Figures 4 and 9 confirms qualitatively equation 8, i.e. the
 278 correlation between the amplitude of gravity wave perturbations and the inverse background
 279 temperature. Quantitatively, in the case of the inbound leg of each orbit, a correlation coeffi-
 280 cient $R \approx 0.70$ between the average of the relative density and the calculated temperature is
 281 found (see Figure 10). Our analysis of the MAVEN is thus compliant with the one conducted
 282 by *Terada et al. [2017]*, and we now turn to the analysis of aerobraking data in the lower ther-
 283 mosphere.



284 **Figure 9.** Seasonal variability of the background temperature estimated from MAVEN/NGIMS density
 285 measurements (ideal gas law and hydrostatic equilibrium). Each point corresponds to the inverse of the mean
 286 background temperature calculated over the outbound leg of each orbit. Data gathered from Martian Year
 287 (MY) 32 are in red, and data from MY33 in blue.



288 **Figure 10.** Correlation between the average of the absolute relative density and the average of the back-
 289 ground temperature calculated for MAVEN/NGIMS data over the inbound leg of each orbit. Temperature is
 290 obtained from the density observations by means of the ideal gas law and the hydrostatic equilibrium

4 Gravity Waves in the Lower Thermosphere: Aerobraking Data

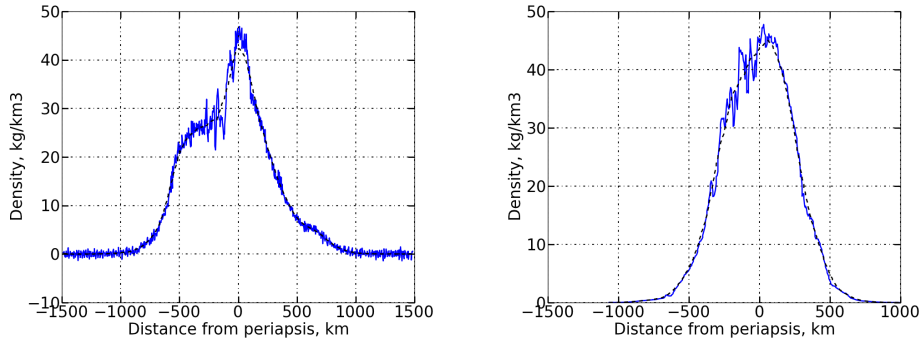
4.1 Analysis

Aerobraking data have been studied in the past to observe the activity of gravity waves in the lower thermosphere, either to discuss the variability of potential sources [Creasey *et al.*, 2006] or to assess wave filtering by zonal jets and how large-amplitude GWs could penetrate to high altitudes [Fritts *et al.*, 2006]. Here we assess if the “inverse temperature” correlation inferred from the MAVEN/NGIMS data [Terada *et al.*, 2017, and section 3 of this paper] can be extended to those lower-thermosphere aerobraking observations obtained by the three accelerometers of MGS, ODY and MRO.

In the aerobraking observations, as is emphasized by Tolson *et al.* [2005] and Tolson *et al.* [2008], the intensity of density perturbations are systematically lower when the spacecraft enters the polar vortex (e.g. MRO during the southern hemisphere winter and ODY during the northern hemisphere winter). Figure 11 shows two examples: ODY orbit 155, which goes through the northern hemisphere winter vortex at $L_s = 298.30^\circ$ and latitude 82.43°N , and MRO orbit 250, going through the southern hemisphere winter vortex at $L_s = 90.01^\circ$ and latitude $=69.50^\circ\text{S}$. These variations of density perturbations within the same orbital track could be explained by the anti-correlation between temperature and gravity wave activity explained above [an explanation that was not provided in Tolson *et al.*, 2008]. Polar warming at thermospheric altitudes [first observed by ODY during aerobraking, Keating *et al.*, 2003] results from the adiabatic heating generated by the subsidence of air over the winter pole produced by strong interhemispheric transport [González-Galindo *et al.*, 2009]. The entry of the spacecraft inside the polar vortex is then expected to be associated with an increase of temperature, leading to a decrease of gravity wave activity according to equation 8.

In Figures 12 and 13, the observed RMS of the relative density variations is compared to the inverse of the background temperature, calculated for each orbit of each instrument over the outbound leg (for the sake of brevity, similar results over the inbound leg are not shown). Latitudinal and seasonal variability are displayed respectively in Figures 12 and 13.

The amplitude of gravity waves present similar features with the inverse of temperature in the MGS observations, with an amplitude increase at latitudes 60°S , 50°N and particularly at 20°S , where inverse temperature is higher in Figure 12, corresponding to $L_s \sim 70^\circ$ in Figure 13. The anti-correlation seems easier to identify in ODY data, in particular at polar latitudes

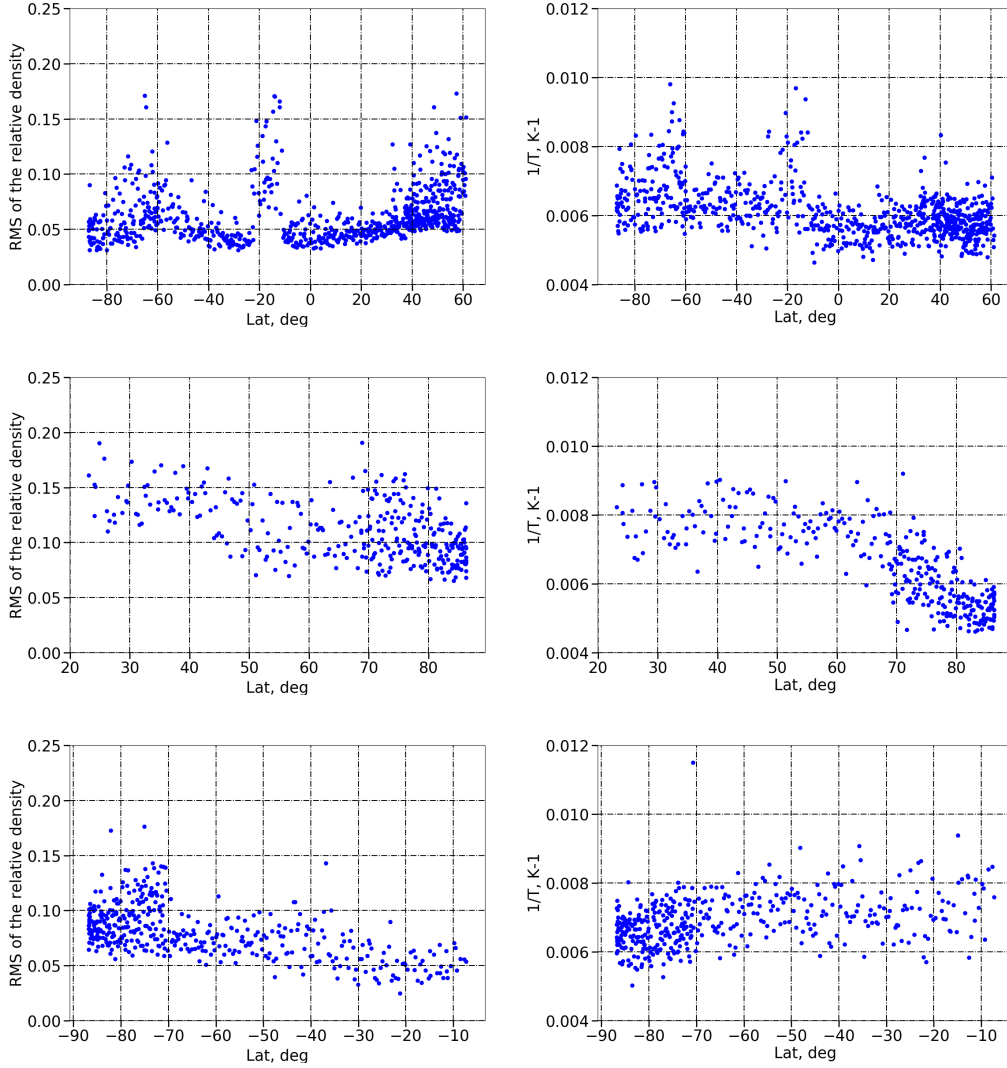


314 **Figure 11.** Examples of orbit 155 of ODY and orbit 250 of MRO. Density variations in kg km^{-3} in func-
 315 tion of the distance from periapsis in km

324 around 80°N , where a clear decrease of GWs amplitude is correlated with the polar warming
 325 (see previous paragraph). Conversely, no obvious correlation between density perturbations
 326 and inverse temperature is found in the MRO aerobraking data: there is an increase in grav-
 327 ity waves activity from latitude -90° to -70° , while the tendency for inverse temperature is
 328 unclear, corresponding to $L_s \sim 35^\circ$ in Figure 13. Furthermore, the gravity waves activity de-
 329 creases at $L_s \sim 95^\circ$, corresponding to a latitude of -20° , whereas it is not the case for inverse
 330 temperature. Correlations have been calculated for the three instruments between the grav-
 331 ity waves amplitude and inverse temperature as done for MAVEN in Figure 10, but for all of
 332 them the correlation coefficient R remains below 0.5. The largest correlation coefficient is
 333 obtained for ODY ($R = 0.48$), whereas it is around 0.2 for the two other datasets.

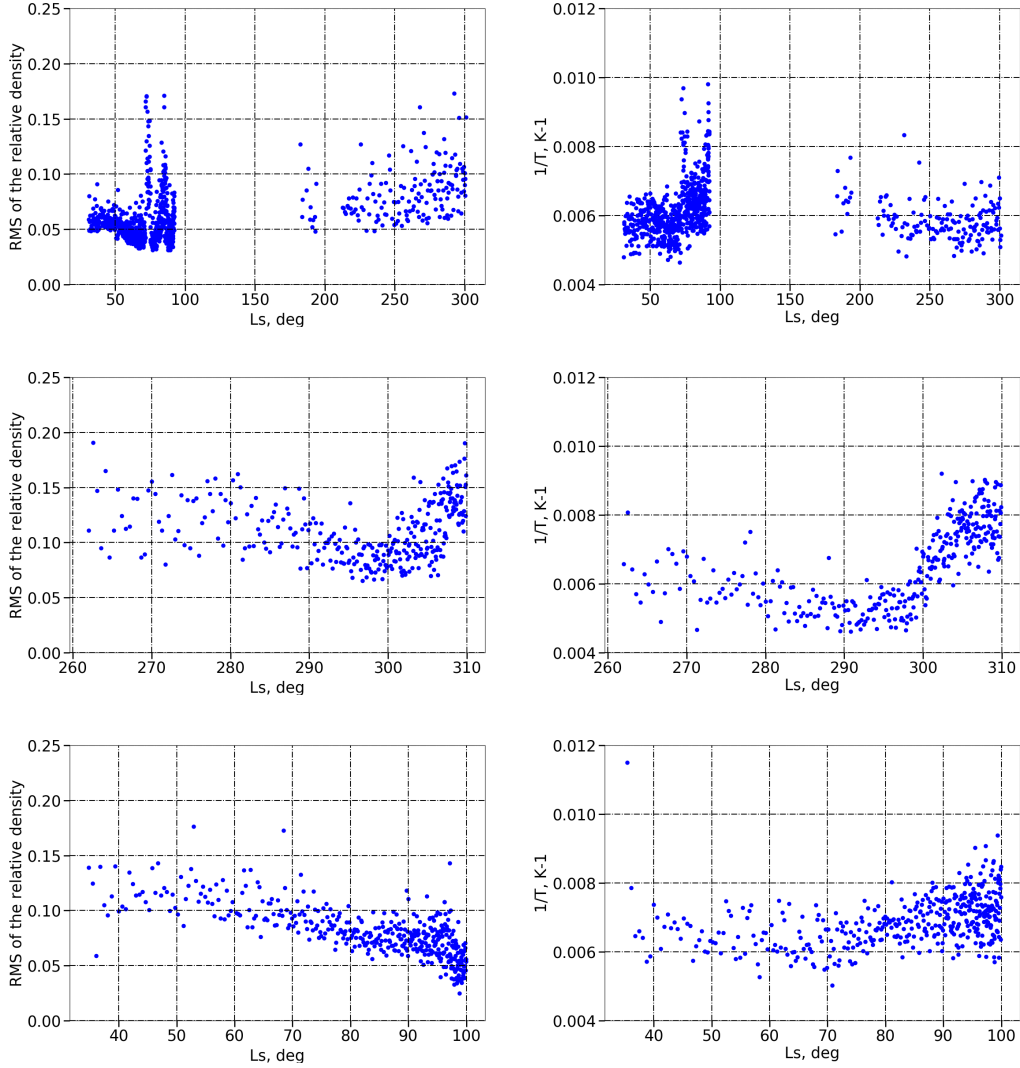
341 4.2 Discussion

342 The correlation between density perturbations, caused by gravity waves, and the in-
 343 verse background temperature, suggested by equation 8, appears to be observed by MAVEN/NGIMS.
 344 A similar correlation, albeit less clear-cut than with the MAVEN/NGIMS dataset, is also
 345 noticed during ODY aerobraking phases at high latitudes. This correlation seems to be ob-
 346 served at certain locations for MGS, as seen in the previous section, and also in particular
 347 cases for MRO, as seen in the previous section for the orbits located in the polar warming.
 348 However, for those two spacecrafts, the correlation is not clear at all in the global analysis of
 349 the complete datasets.



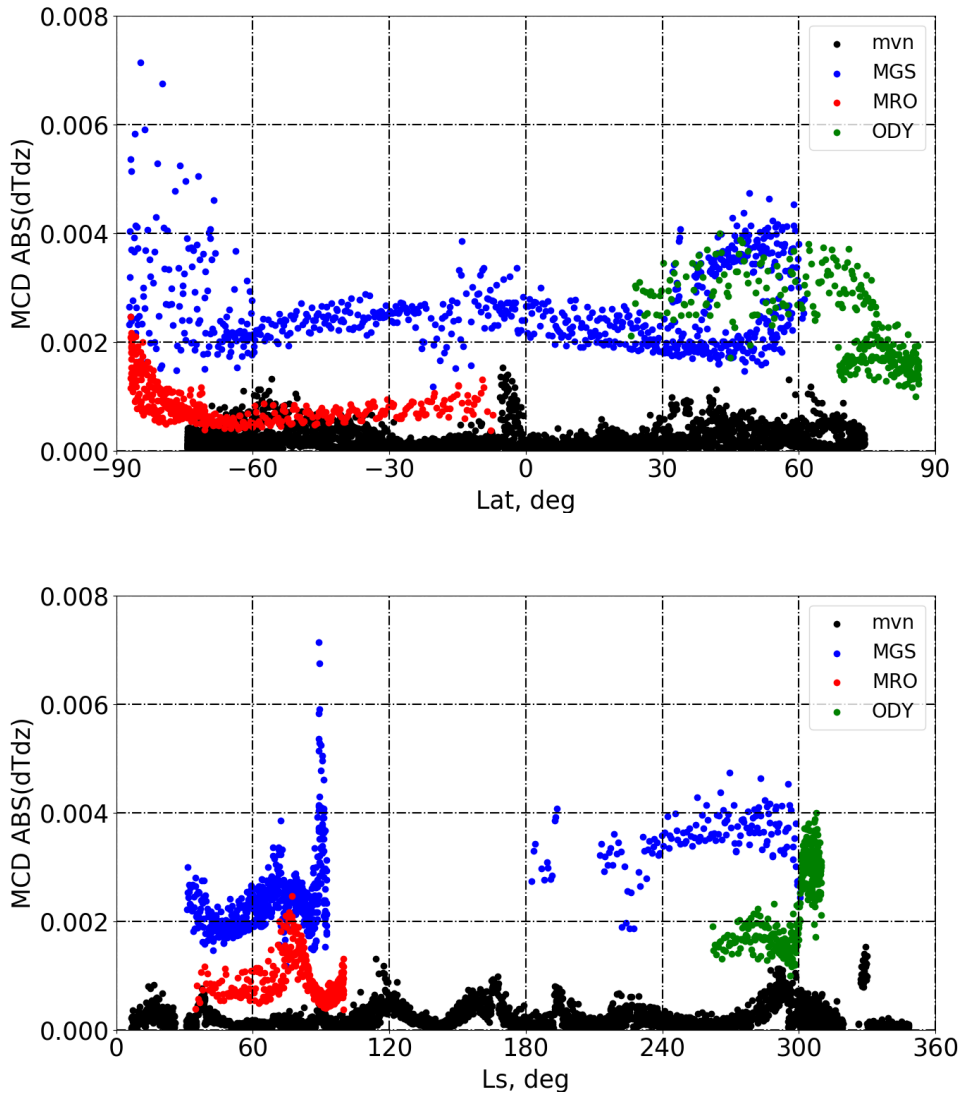
334 **Figure 12.** From the upper to the lower: MGS, ODY, MRO. From the left to the right: RMS of the relative
 335 density calculated over the outbound leg according to the latitude of the orbit's periapsis, inverse of the mean
 336 background temperature calculated from the observations over the outbound leg according to the latitude of
 337 the orbit's periapsis

350 The aerobraking density measurements correspond to periapsis conditions at lower
 351 altitudes than the MAVEN/NGIMS measurements (cf. Figure 1). There, the assumption of
 352 isothermal profiles could not be valid. Indeed, in Figure 14 we compare the temperature gra-
 353 dients calculated with the MCD for the three aerobraking missions along with MAVEN/NGIMS.
 354 The Figure shows that MAVEN/NGIMS data mainly correspond to isothermal profiles, whereas
 355 the three other instruments present larger temperature gradients. Yet, equation 8 is only ef-
 356 fective in isothermal conditions. As a matter of fact, we observe in the ODY data that a po-



338 **Figure 13.** From the upper to the lower: MGS, ODY, MRO. From the left to the right: RMS of the rela-
 339 tive density calculated over the outbound leg according to L_s , inverse of the mean background temperature
 340 calculated from the observations over the outbound leg according to L_s

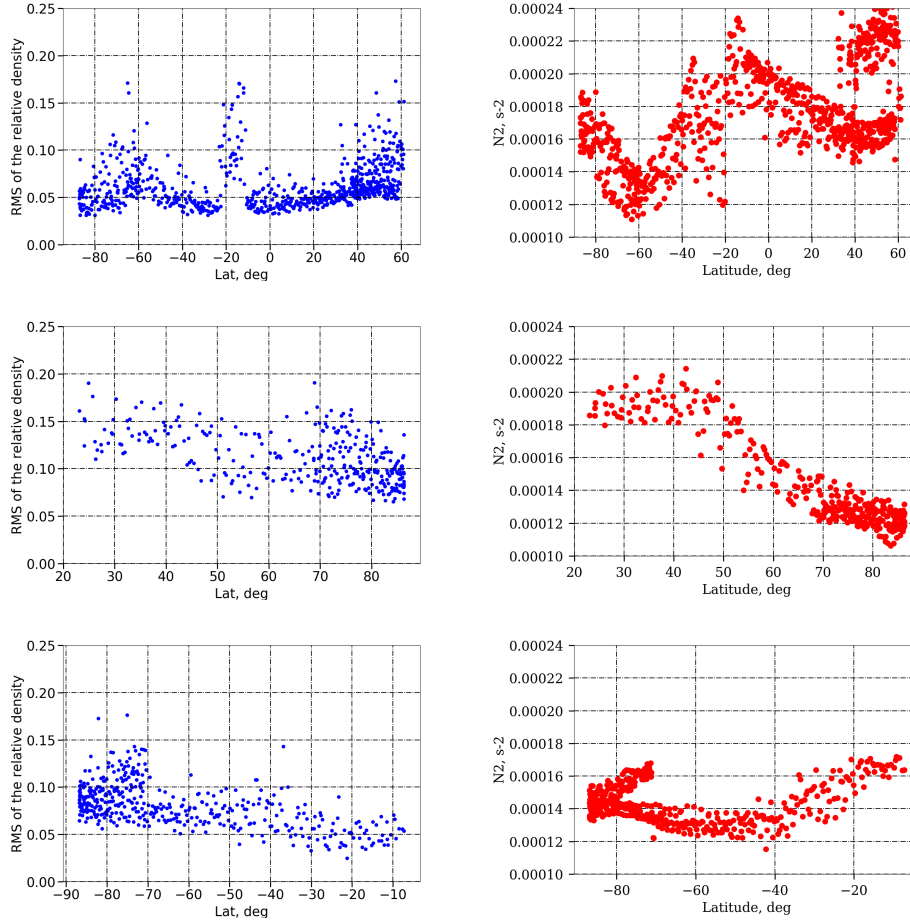
357 potential correlation between gravity wave activity and inverse temperature only appears where
 358 the temperature gradient is the lowest, at higher latitudes. This is also possibly the case for
 359 MGS at the points located around latitudes -60° and -20° . However, MRO, which presents
 360 the lowest temperature gradient, presents no clear correlation with the inverse temperature.
 361 There could be an explanation for the temperature gradient being lower for ODY and MRO,
 362 despite the fact they are lower in altitude: at polar latitudes, the polar warming shifts the
 363 threshold for isothermal conditions to lower altitudes in the mesosphere. Furthermore, when
 364 the temperature gradient is significant, the more general equation 6 shall prevail instead of



367 **Figure 14.** Upper: Absolute value of the mean temperature gradient along the latitude calculated with the
 368 MCD over the outbound leg of each orbit of the different aerobraking instruments and MAVEN/NGIMS.
 369 Down: Absolute value of the mean temperature gradient along the L_s calculated with the MCD over the
 370 outbound leg of each orbit of the different aerobraking instruments and MAVEN/NGIMS.

365 equation 8, which means that the amplitude of gravity waves is proportional to the static sta-
 366 bility N^2 rather than the inverse background temperature.

371 The possible correlation with static stability N^2 can be tested with the MCD in the con-
 372 ditions that were met by the aerobraking measurements. Figure 15 displays the comparison
 373 between the RMS of the relative density acquired at the different aerobraking orbits and the



381 **Figure 15.** From the upper to the lower: MGS, ODY, MRO. Left : RMS of the relative density calculated
 382 over the outbound leg of each orbit of aerobraking data according to the latitude of the orbit's periapsis ; Right
 383 : Mean static stability N^2 calculated over the outbound leg of each orbit of aerobraking data according to the
 384 latitude of the orbit's periapsis, N^2 has been calculated by means of the Mars Climate Database (MCD) at the
 385 different orbital characteristics and with the corresponding dedicated MCD dust scenarios of Mars Year (MY)
 386 25 (MCD detailed document, *Montabone et al.* [2015])

374 static stability calculated from the MCD (for the corresponding orbital spatio-temporal co-
 375 ordinates). We observe the same peak of gravity waves activity and static stability for MGS
 376 at latitude -20° and in the North pole, but not for the other latitudes. A good correlation be-
 377 tween the GWs activity and the static stability, as with the inverse temperature, can be found
 378 for ODY. Regarding MRO, the static stability N^2 correlates well to the observed amplitude of
 379 gravity waves in high-latitude regions (latitudes above -50°S), but such a correlation is not
 380 found at lower latitudes.

387 There might be multiple reasons for aerobraking measurements not following equa-
388 tion 6 in the low and mid latitudes. Firstly, while no correlation was found with potential
389 sources of gravity wave, it is still possible that outside the polar regions, propagation effects
390 would compete with the regional variability of gravity-wave sources. Secondly, following
391 a similar argument, the filtering by critical levels was ruled out for a lack of clear tendency,
392 but might be of peculiar importance for specific regions [see *Spiga et al.*, 2012]. Thirdly,
393 the regional variability of vertical wavelength k_z , a parameter found in equations 6 and 8, in
394 principle could impact density perturbations [*Smith et al.*, 1987], which then would be less
395 clearly correlated to static stability N^2 .

396 5 Conclusion

397 We have studied the seasonal and regional variability of density perturbations, puta-
398 tively caused by the propagation of gravity waves in the thermosphere, in different sets of
399 data issued from the aerobraking phases of MGS, ODY and MRO (accelerometers) and the
400 observations of the NGIMS instrument on board MAVEN. The modeling compiled in the
401 Mars Climate Database has been used to complement background atmospheric conditions
402 obtained by observations. Our conclusions are as follows:

- 403 1. The correlation found in the MAVEN observations by *Terada et al.* [2017] between
404 the inverse background temperature and the density perturbations reasonably extends
405 to the ODY aerobraking measurements, but not to the MGS and MRO aerobraking
406 measurements. This result emphasizes the exceptional nature of MAVEN datasets,
407 which combine both isothermal and saturated conditions (equation 8). The seasonal
408 variability of inverse background temperature measured by MAVEN is reproduced in
409 the Mars Climate Database.
- 410 2. In comparison to MAVEN/NGIMS measurements, MGS, ODY and MRO aerobrak-
411 ing data cover a lower layer in the thermosphere, where the Mars Climate Database
412 predicts non-isothermal conditions. In these conditions, and under the hypothesis of
413 saturation, a correlation between the gravity waves perturbation with the static stabil-
414 ity is expected (equation 6). A correlation of density perturbations monitored both
415 by ODY and MRO during aerobraking in polar regions with static stability N^2 is ob-
416 served and indicates that wave saturation might be still dominant, but the isothermal
417 conditions are no longer verified (equation 6).

418 3. The spatial variability of gravity-wave-induced density perturbations are difficult to
419 explain for the global MGS dataset and in lower latitudes for ODY and MRO aero-
420 braking, where no clear correlation with neither inverse temperature nor static sta-
421 bility is found. The effects of gravity-wave sources, or wind filtering effects through
422 critical levels, were ruled out as explanations for most of the measured variability, yet
423 might play a stronger role in the low-to-mid latitudes.

424 Future studies will employ measurements during the aerobraking phase of the ExoMars
425 Trace Gas Orbiter, as well as new measurements by MAVEN, to confirm the conclusions
426 drawn in this study and the existing literature. Broadening the knowledge of gravity wave
427 activity in the mesosphere and thermosphere is crucial to understand the large-scale heat and
428 momentum budget of this part of the Martian atmosphere.

429 **Acknowledgments**

430 The authors acknowledge Centre National d'Études Spatiale (CNES) and European Space
431 Agency (ESA) for financial support. We thank two reviewers for thorough and constructive
432 comments that helped us to improve this paper.

433 **References**

- 434 Alexander, M. J., M. Geller, C. McLandress, S. Polavarapu, P. Preusse, F. Sassi, K. Sato,
435 S. Eckermann, M. Ern, A. Hertzog, Y. Kawatani, M. Pulido, T. A. Shaw, M. Sigmond,
436 R. Vincent, and S. Watanabe (2010), Recent developments in gravity-wave effects in cli-
437 mate models and the global distribution of gravity-wave momentum flux from observa-
438 tions and models, *Quarterly Journal of the Royal Meteorological Society*, 136(650), 1103–
439 1124, doi:10.1002/qj.637.
- 440 Barnes, J. R. (1990), Possible effect of breaking gravity waves on the circulation of the mid-
441 dle atmosphere of Mars, *J. Geophys. Res.*, 95, 1401–1421.
- 442 Benna, M., and E. Lyness (2014), MAVEN Neutral Gas and Ion Mass Spectrometer Data,
443 urn:nasa:pds:maven_ngims.
- 444 Bougher, S. W., R. G. Roble, E. C. Ridley, and R. E. Dickinson (1990), The Mars thermo-
445 sphere. II - General circulation with coupled dynamics and composition, *J. Geophys. Res.*,
446 95, 14,811–14,827.

- 447 Briggs, G. A., and C. B. Leovy (1974), Mariner 9 observations of the Mars north polar hood,
448 *Bull. Am. Meteorol. Soc.*, *55*, 278–296.
- 449 Collins, M., S. Lewis, and P. L. Read (1997), Gravity wave drag in a global circulation model
450 of the Martian atmosphere: parametrisation and validation, *Adv. Space Res.*, *44*, 1395–
451 1409.
- 452 Creasey, J. E., J. M. Forbes, and G. M. Keating (2006), Density variability at scales typi-
453 cal of gravity waves observed in Mars' thermosphere by the MGS accelerometer, *Geo-*
454 *phys. Res. Lett.*, *33*, L22,814, doi:10.1029/2006GL027583.
- 455 Eckermann, S. D., J. Ma, and X. Zhu (2011), Scale-dependent infrared radiative damping
456 rates on Mars and their role in the deposition of gravity-wave momentum flux, *211*, 429–
457 442, doi:10.1016/j.icarus.2010.10.029.
- 458 England, S. L., G. Liu, E. Yiğit, P. R. Mahaffy, M. Elrod, M. Benna, H. Nakagawa, N. Ter-
459 ada, and B. Jakosky (2017), MAVEN NGIMS observations of atmospheric gravity waves
460 in the Martian thermosphere, *Journal of Geophysical Research (Space Physics)*, *122*,
461 2310–2335.
- 462 Forget, F., F. Hourdin, R. Fournier, C. Hourdin, O. Talagrand, M. Collins, S. R. Lewis, P. L.
463 Read, and J.-P. Huot. (1999), Improved general circulation models of the Martian atmo-
464 sphere from the surface to above 80 km, *J. Geophys. Res.*, *104*, 24,155–24,176.
- 465 Fritts, D., and M. Alexander (2003), Gravity wave dynamics and effects in the middle atmo-
466 sphere, *Rev. Geophys.*, *41*(1), 1003.
- 467 Fritts, D. C., L. Wang, and R. H. Tolson (2006), Mean and gravity wave structures and
468 variability in the Mars upper atmosphere inferred from Mars Global Surveyor and Mars
469 Odyssey aerobraking densities, *Journal of Geophysical Research (Space Physics)*,
470 *111*(A10), 12,304–+, doi:10.1029/2006JA011897.
- 471 Gilli, G., F. Forget, A. Spiga, T. Navarro, and M. T. (2018), Impact of gravity waves on the
472 middle atmosphere of mars: a non-orographic gravity wave parameterization based on
473 global climate modeling and mcs observations, Submitted to *Journal of Geophysical Re-*
474 *search*.
- 475 González-Galindo, F., F. Forget, M. A. López-Valverde, and M. Angelats i Coll (2009), A
476 Ground-to-Exosphere Martian General Circulation Model. 2. The Atmosphere During
477 Perihelion Conditions: Thermospheric Polar Warming , *Journal of Geophysical Research*
478 *(Planets)*, *114*(E13), E08,004, doi:10.1029/2008JE003277.

- 479 Gossard, E. E., and W. H. Hooke (1975), *Waves in the atmosphere: Atmospheric infrasound*
480 *and gravity waves - Their generation and propagation, Developments in Atmospheric Sci-*
481 *ence*, vol. 2, first ed., Elsevier Scientific Publishing.
- 482 Hartogh, P., A. S. Medvedev, T. Kuroda, R. Saito, G. Villanueva, A. G. Feofilov, A. A.
483 Kutepov, and U. Berger (2005), Description and climatology of a new general circulation
484 model of the Martian atmosphere, *Journal of Geophysical Research (Planets)*, *110*(E9),
485 11,008, doi:10.1029/2005JE002498.
- 486 Hauchecorne, A., M. L. Chanin, and R. Wilson (1987), Mesospheric tempera-
487 ture inversion and gravity wave breaking, *Geophys. Res. Lett.*, *14*, 933–936, doi:
488 10.1029/GL014i009p00933.
- 489 Imamura, T., A. Watanabe, and Y. Maejima (2016), Convective generation and vertical prop-
490 agation of fast gravity waves on Mars: One- and two-dimensional modeling, *Icarus*, *267*,
491 51–63, doi:10.1016/j.icarus.2015.12.005.
- 492 Jakosky, B. M., R. P. Lin, J. M. Grebowsky, J. G. Luhmann, D. F. Mitchell, G. Beutelschies,
493 T. Priser, M. Acuna, L. Andersson, D. Baird, D. Baker, R. Bartlett, M. Benna, S. Bougher,
494 D. Brain, D. Carson, S. Cauffman, P. Chamberlin, J.-Y. Chaufray, O. Cheatom, J. Clarke,
495 J. Connerney, T. Cravens, D. Curtis, G. Delory, S. Demcak, A. DeWolfe, F. Eparvier,
496 R. Ergun, A. Eriksson, J. Espley, X. Fang, D. Folta, J. Fox, C. Gomez-Rosa, S. Habenicht,
497 J. Halekas, G. Holsclaw, M. Houghton, R. Howard, M. Jarosz, N. Jedrich, M. Johnson,
498 W. Kasprzak, M. Kelley, T. King, M. Lankton, D. Larson, F. Leblanc, F. Lefevre, R. Lil-
499 lis, P. Mahaffy, C. Mazelle, W. McClintock, J. McFadden, D. L. Mitchell, F. Montmessin,
500 J. Morrissey, W. Peterson, W. Possel, J.-A. Sauvaud, N. Schneider, W. Sidney, S. Spira-
501 cino, A. I. F. Stewart, R. Tolson, D. Toubanc, C. Waters, T. Woods, R. Yelle, and R. Zurek
502 (2015), The Mars Atmosphere and Volatile Evolution (MAVEN) Mission, *Space Science*
503 *Reviews*, *195*, 3–48, doi:10.1007/s11214-015-0139-x.
- 504 Keating, G., R. Tolson, J. Hanna, R. Beebe, J. Murphy, and L. Huber (2002), MGS-M-
505 ACCEL-5-PROFILE-V1.2, NASA Planetary Data System.
- 506 Keating, G. M., M. Theriot, Jr., R. Tolson, S. Bougher, F. Forget, and J. Forbes (2003),
507 Global Measurements of the Mars Upper Atmosphere: In Situ Accelerometer Measure-
508 ments from Mars Odyssey 2001 and Mars Global Surveyor, in *Lunar and Planetary Insti-*
509 *tute Conference Abstracts*, edited by S. Mackwell and E. Stansbery, p. 1142.
- 510 Lewis, S. R., M. Collins, P. L. Read, F. Forget, F. Hourdin, R. Fournier, C. Hourdin, O. Tala-
511 grand, and J.-P. Huot. (1999), A climate database for Mars, *J. Geophys. Res.*, *104*, 24,177–

512 24,194.

513 Lindzen, R. S. (1981), Turbulence and stress owing to gravity wave and tidal breakdown,
514 *J. Geophys. Res.*, *86*, 9707–9714.

515 Lyons, D. T., J. G. Beerer, P. Esposito, M. D. Johnston, and W. H. Willcockson (1999), Mars
516 Global Surveyor: Aerobraking Mission Overview, *Journal of Spacecraft and Rockets*, *36*,
517 307–313, doi:10.2514/2.3472.

518 Mahaffy, P. R., M. Benna, M. Elrod, S. W. Bougher, R. Yelle, and B. M. Jakosky (2015),
519 Early Composition, Structure, and Isotope Measurements in the Upper Atmosphere of
520 Mars from MAVEN’s Neutral Gas and Ion Mass Spectrometer, in *Lunar and Planetary
521 Science Conference, Lunar and Planetary Science Conference*, vol. 46, p. 1981.

522 McFarlane, N. A. (1987), The effect of orographically excited gravity wave drag on the gen-
523 eral circulation of the lower stratosphere and troposphere, *J. Atmos. Sci.*, *44*, 1775–1800.

524 Medvedev, A. S., F. González-Galindo, E. Yiğit, A. G. Feofilov, F. Forget, and P. Hartogh
525 (2015), Cooling of the Martian thermosphere by CO₂ radiation and gravity waves: An
526 intercomparison study with two general circulation models, *Journal of Geophysical Re-
527 search (Planets)*, *120*, 913–927, doi:10.1002/2015JE004802.

528 Millour, E., F. Forget, A. Spiga, T. Navarro, J.-B. Madeleine, L. Montabone, A. Pottier,
529 F. Lefevre, F. Montmessin, J.-Y. Chaufray, M. A. Lopez-Valverde, F. Gonzalez-Galindo,
530 S. R. Lewis, P. L. Read, J.-P. Huot, M.-C. Desjean, and MCD/GCM development Team
531 (2015), The Mars Climate Database (MCD version 5.2), *European Planetary Science
532 Congress 2015, 10*, EPSC2015–438.

533 Montabone, L., F. Forget, E. Millour, R. J. Wilson, S. R. Lewis, B. Cantor, D. Kass,
534 A. Kleinböhl, M. T. Lemmon, M. D. Smith, and M. J. Wolff (2015), Eight-year climatol-
535 ogy of dust optical depth on Mars, *Icarus*, *251*, 65–95, doi:10.1016/j.icarus.2014.12.034.

536 O’sullivan, D., and T. Dunkerton (1995), Generation of Inertia–Gravity Waves in a Simulated
537 Life Cycle of Baroclinic Instability, *Journal of the Atmospheric Sciences*, *52*(21), 3695–
538 3716.

539 Palmer, T. N., G. J. Shutts, and R. Swinbank (1986), Alleviation of a systematic westerly bias
540 in general circulation and numerical weather prediction models through an orographic
541 gravity wave drag parametrisation, *Q. J. R. Meteorol. Soc.*, *112*, 1001–1039.

542 Parish, H. F., G. Schubert, M. P. Hickey, and R. L. Walterscheid (2009), Propagation of
543 tropospheric gravity waves into the upper atmosphere of Mars, *Icarus*, *203*, 28–37, doi:
544 10.1016/j.icarus.2009.04.031.

- 545 Pickersgill, A. O., and G. E. Hunt (1979), The formation of Martian lee waves generated by a
546 crater, *J. Geophys. Res.*, *84*(B14), 8317–8331.
- 547 Pickersgill, A. O., and G. E. Hunt (1981), An examination of the formation of linear lee
548 waves generated by giant Martian volcanoes, *J. Atmos. Sci.*, *38*, 40–51.
- 549 Plougonven, R., H. Teitelbaum, and V. Zeitlin (2003), Inertia gravity wave generation by the
550 tropospheric midlatitude jet as given by the Fronts and Atlantic Storm-Track Experiment
551 radio soundings, *J. Geophys. Res.*, *108*(21), 4686–4704, doi:10.1029/2003JD003535.
- 552 Siddle, A., I. Mueller-Wodarg, S. Stone, and R. Yelle (2019), Global characteristics of grav-
553 ity waves in the upper atmosphere of Mars as measured by MAVEN/NGIMS, *Icarus*, *333*,
554 12–21, doi:10.1016/j.icarus.2019.05.021.
- 555 Smith, J. C., and J. Bell (2005), 2001 Mars Odyssey Aerobraking, *Journal of Spacecraft and*
556 *Rockets*, *42*, 406–415, doi:10.2514/1.15213.
- 557 Smith, S. A., D. C. Fritts, and T. E. Vanzandt (1987), Evidence for a Saturated Spectrum of
558 Atmospheric Gravity Waves., *Journal of Atmospheric Sciences*, *44*(10), 1404–1410, doi:
559 10.1175/1520-0469(1987)044<1404:EFASSO>2.0.CO;2.
- 560 Spiga, A., H. Teitelbaum, and V. Zeitlin (2008), Identification of the sources of inertia-
561 gravity waves in the Andes Cordillera region, *Annales Geophysicae*, *26*, 2551–2568.
- 562 Spiga, A., F. González-Galindo, M.-Á. López-Valverde, and F. Forget (2012), Gravity waves,
563 cold pockets and CO₂ clouds in the Martian mesosphere, *Geophys. Res. Letters*, *39*,
564 L02201, doi:10.1029/2011GL050343.
- 565 Spiga, A., J. Faure, J.-B. Madeleine, A. Määttänen, and F. Forget (2013), Rocket dust storms
566 and detached dust layers in the Martian atmosphere, *Journal of Geophysical Research*
567 *(Planets)*, *118*, 746–767, doi:10.1002/jgre.20046.
- 568 Terada, N., F. Leblanc, H. Nakagawa, A. S. Medvedev, E. Yiğit, T. Kuroda, T. Hara, S. L.
569 England, H. Fujiwara, K. Terada, K. Seki, P. R. Mahaffy, M. Elrod, M. Benna, J. Gre-
570 bowsky, and B. M. Jakosky (2017), Global distribution and parameter dependences of
571 gravity wave activity in the Martian upper thermosphere derived from MAVEN/NGIMS
572 observations, *Journal of Geophysical Research (Space Physics)*, *122*, 2374–2397.
- 573 Tolson, R. (2007), MRO Profile Data Records V1.0, MRO-M-ACCEL-2-PROFILE-V1.0,
574 NASA Planetary Data System.
- 575 Tolson, R., A. M. Dwyer, P. E. Escalera, B. E. George, J. L. Hanna, G. M. Keating, and
576 M. R. Werner (2005), Application of Accelerometer Data to Mars Odyssey Aerobrak-
577 ing and Atmospheric Modeling, *Journal of Spacecraft and Rockets*, *42*, 435–443, doi:

- 578 10.2514/1.15173.
- 579 Tolson, R., J. Murphy, R. Beebe, and L. Huber (2007a), ODY-M-ACCEL-5-PROFILE-V2.0,
580 NASA Planetary Data System.
- 581 Tolson, R., E. Bemis, S. Hough, K. Zaleski, G. Keating, J. Shidner, S. Brown, A. Brick-
582 ler, M. Scher, and P. Thomas (2008), Atmospheric Modeling Using Accelerometer Data
583 During Mars Reconnaissance Orbiter Aerobraking Operations, *Journal of Spacecraft and*
584 *Rockets*, 45, 511–518, doi:10.2514/1.34301.
- 585 Tolson, R. H., G. J. Cancro, G. M. Keating, S. N. Noll, J. S. Parker, and B. L. Wilkerson
586 (1999), Application of Accelerometer Data to Mars Global Surveyor Aerobraking Oper-
587 ations, *Journal of Spacecraft and Rockets*, 36, 323–329, doi:10.2514/2.3474.
- 588 Tolson, R. H., G. M. Keating, R. W. Zurek, S. W. Bougher, C. G. Justus, and D. C. Fritts
589 (2007b), Application of Accelerometer Data to Atmospheric Modeling During Mars
590 Aerobraking Operations, *Journal of Spacecraft and Rockets*, 44, 1172–1179, doi:
591 10.2514/1.28472.
- 592 Vincent, R. A., and M. J. Alexander (2000), Gravity waves in the tropical lower stratosphere:
593 An observational study of seasonal and interannual variability, *J. Geophys. Res.*, 105(14),
594 17,971–17,982, doi:10.1029/2000JD900196.
- 595 Yiğit, E., S. L. England, G. Liu, A. S. Medvedev, P. R. Mahaffy, T. Kuroda, and B. M.
596 Jakosky (2015), High-altitude gravity waves in the martian thermosphere observed by
597 maven/ngims and modeled by a gravity wave scheme, *Geophysical Research Letters*, pp. –,
598 doi:10.1002/2015GL065307, 2015GL065307.